Proceedings of the 21st ICSMGE, Vienna, Austria, 14 – 19 June 2026. Pistrol, Adam & Schweiger (eds.)
Published by: ÖGG, Austrian Society for Geomechanics, Salzburg, Austria, ISBN 978-3-9503898-4-5
https://doi.org/10.53243/ICSMGE2026-607

Analysis of the amplification factor for linear seismic response in a two-dimensional homogeneous V-shaped site

Haowei Yang, Jie Cui, Wei Zhang, Yadong Li, Yi Shan
School of Civil Engineering and Transportation, Guangzhou University, Guangzhou, China, yangssi1987@126.com

Pengfei Dang
School of Civil & Environmental Engineering and Geography Science, Ningbo University, Ningbo, China

ABSTRACT: Ground motion during an earthquake is significantly influenced by site effects during its propagation. To quantify the site amplification effect of a valley site, key geometric parameters, such as slope height and shape ratio, as well as mechanical parameters, such as shear wave velocity and seismic wave frequency, were considered as influencing factors. A total of 768 numerical models were developed, and finite element analysis was performed. Numerical analysis reveals that ground motion amplification on the surface of V-shaped river valleys is most pronounced at the slope crest, with the effect intensifying as the shape ratio increases, shear wave velocity decreases, and frequency ratio rises. Terrain geometry, material properties, and seismic wave frequency collectively influence the amplification factor, with frequency ratio exerting the most significant effect. The polynomial fitting method used to develop the amplification factor formula for V-shaped sites demonstrates strong agreement with numerical simulation results and, while slightly underestimating observed values, accurately captures the overall trend. This indicates both statistical reliability and practical engineering applicability. Comparison with domestic and international codes shows that current standards do not fully account for the influence of seismic wave frequency, which results in the underestimation of the amplification factor at the edges of V-shaped sites. The findings of this study provide a robust theoretical foundation and methodological guidance for seismic hazard assessment and seismic design in areas characterized by complex terrain.

KEYWORDS: Geotechnical earthquake engineering, Two-dimensional site effects, Linear seismic response, Amplification factor, Seismic wave frequency.

1 INTRODUCTION

Alluvial valleys have historically served as important centers for human settlement, primarily due to their advantageous transportation routes and abundant water resources. However, these regions are particularly vulnerable to seismic hazards, as the amplification of ground motion by valley terrain significantly increases seismic risk. Numerous post-earthquake investigations have revealed pronounced spatial variability in seismic damage within alluvial basins. Traditional stratigraphic effects alone cannot fully account for this observed non-uniformity (Alleanza et al. 2024; Cetin et al. 2023).

Previous studies have demonstrated that complex seismic wave interactions within basins—including reflection, refraction, and surface wave trapping—can substantially amplify ground motion (Amini et al. 2022; Ba et al. 2024). Despite these insights, there remains a lack of effective methods to quantitatively assess the influence of geometric and mechanical parameters on terrain amplification, which limits the refinement of seismic design codes.

To address this research gap, the present study employs a parametric analysis approach to investigate the amplification effects associated with V-shaped valley topography. Utilizing finite element numerical simulations, a comprehensive model system comprising 768 scenarios was developed. The analysis focuses on the impact of key parameters, including slope height, shape ratio, shear wave velocity, and seismic wave frequency. The findings aim to establish a predictive model for the terrain amplification factor in V-shaped river valleys, thereby providing a theoretical basis to enhance seismic design practices in such environments.

2 MODEL AND METHOD

2.1 *Viscoelastic artificial boundaries and equivalent nodal forces*

In the analysis of near-field seismic wave propagation, it is standard practice to introduce truncated computational domains with non-reflecting boundaries. These artificial absorbing boundaries enable outgoing waves to pass through, thereby minimizing artificial reflections and accurately simulating wave transmission to the far field. A commonly used approach is the viscous spring boundary, which is physically represented by a series of spring-damper elements connected to the boundary nodes. The elastic spring coefficient (K) and damping coefficient (C) for these boundaries are defined as follows:

$$\begin{cases} K_N = \dfrac{1}{1+a}\dfrac{\lambda+2G}{2r}, \quad C_N = b\rho c_{\mathrm{p}} \\ K_T = \dfrac{1}{1+a}\dfrac{G}{2r}, \quad C_T = b\rho c_{\mathrm{s}} \end{cases} \tag{1}$$

Where, the subscripts N and T denote the normal and tangential directions, respectively. Here, λ is the first Lamé parameter, G is the shear modulus, and r represents the distance between the wave source and the artificial boundary. The terms c_{p} and c_{s} correspond to the compressional and shear wave velocities in the medium, respectively. The coefficients a and b are dimensionless, with recommended values of 0.8 and 1.1, respectively.

According to Jingbo et al. (2023), seismic waves can be transformed into equivalent node forces at the model boundary nodes. Through derivation, the expression of the equivalent node force at the boundary node l can be obtained as shown in Eq. (2).

$$F_{li} = \left(K_{li}u_{li}^{f} + C_{li}\dot{u}_{li}^{f} + \sigma_{li}^{f}\right)A_l \tag{2}$$

Where, m denotes the lumped mass at the boundary node, while c and k represent the damping and stiffness coefficients, respectively. The term A refers to the influence area associated with all elements surrounding the node.

2.2 *Numerical model*

In this study, two-dimensional numerical simulations were performed using the ABAQUS finite element software. The model, illustrated in Figure 2, represents a homogeneous V-shaped site. To simulate a semi-infinite foundation and effectively absorb the energy of scattered waves, viscoelastic artificial boundaries were applied at the base and lateral edges

of the model. Seismic loading was introduced by vertically incident SV waves from the bottom, representing far-field seismic excitation. The computational mesh consists of quadrilateral elements, with the maximum element size set to one-tenth of the minimum propagation wavelength, in accordance with the Kuhlemeyer and Lysmer criteria (Kuhlemeyer & Lysmer. 1973). As shown in Figure 1, the prototype valley site located in Sichuan Province, China (Li et al. 2022), has a slope height of 120 m and a shape ratio of 0.4. For the parametric study, based on this prototype site, the numerical valley models were assigned slope heights (h) of 50, 100, 200, and 400 m, and shape ratios (h/l) of 0.25, 0.5, 1, and 2. The total height of the model is 3h. Shear wave velocities (vs) were selected as 400, 700, 1000, and 1300 m/s, following the (GB50011-2010), corresponding to damping ratios of 2%, 1.5%, 1%, and 0.5%, respectively. These values encompass a range of site conditions, including rock, hard soil, and medium-hard soil, all under small-strain conditions. Rayleigh damping was adopted for the viscoelastic half-space. To investigate frequency effects, the frequency ratio (f_m/f_{1D}) was set to 8, 6, 4, 2, 1, and 0.5, where f_m is the predominant frequency of the Ricker wave and f_{1D} is the fundamental site frequency (Eq.(3)). The detailed model parameters are summarized in Table 1.

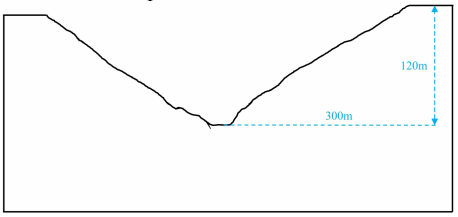

Figure 1. Slope profile of the actual river-valley site.

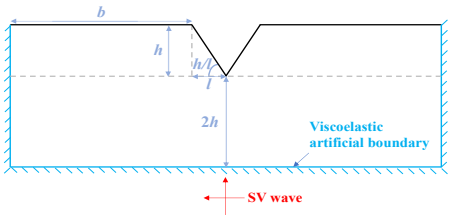

Figure 2. Two-dimensional homogeneous V-shaped site model.

$$f_{1D} = \frac{vs}{4z} \tag{3}$$

Where, vs represents the shear wave velocity of the soil mass, and z represents the depth of the soil layer.

Table 1. Model parameters.

h (m)	h/l	vs (m/s)	f_m/f_{1D}
50	0.25	400	0.5
100	0.5	700	1
200	1	1000	2
400	2	1300	4
			6
			8

A set of eight Ricker waveforms was used as the acceleration input for ground motion, denoted as $a(t)$, to analyze the influence of frequency content. The analytical expression for the Ricker wave is provided in Eq.(4). Figure 3 presents the acceleration time histories for all input motions, plotted against the normalized time variable ($t \times f_m$), where t is the time and (f_m) is the predominant frequency.

$$a(t) = PGA \cdot \left\{1 - 2 \cdot \left[\pi \cdot f_m \cdot (t - t_0)\right]^2\right\} \cdot e^{-\left[\pi \cdot f_m \cdot (t - t_0)\right]^2} \tag{4}$$

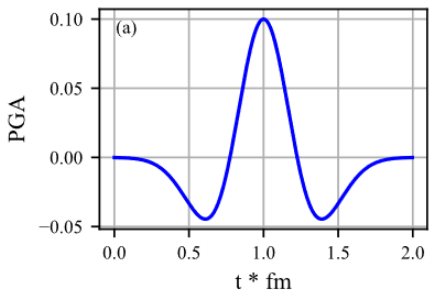

Figure 3. Ricker wavelet acceleration normalized time-history curve.

3 RESULTS AND ANALYSIS

3.1 *The influence law of influencing factors on the amplification effect of V-shaped river valleys*

A total of 768 two-dimensional analyses were performed by systematically combining 16 geometric models (derived from four shape ratios and four slope heights, as detailed in Table 1), four shear wave velocities (Table 1), and six input motions (Table 1). For each configuration, a corresponding two-dimensional flat free-field model was also established. To accurately assess terrain amplification effects, this study adopted the normalized peak acceleration metric proposed, referred to as the Terrain Amplification Factor (TAF) (Assimaki et al. 2005). TAF is defined as the ratio of the peak ground acceleration (PGA) at the ground surface to the horizontal PGA of the free-field (Eq. (5)). This approach effectively isolates geometric effects—those attributable to topography—from stratigraphic effects associated with vertical soil layering. As a result, the analysis provides a clearer understanding of how site geometry amplifies ground motion during seismic events, independent of the influence of subsurface strata.

$$TAF = \frac{a_{h,\max}}{a_{h,\mathrm{ff}}} \tag{5}$$

Where, $a_{h,\max}$ represents the horizontal PGA on the ground, and $a_{h,\mathrm{ff}}$ represents the horizontal PGA in the free field.

To systematically investigate the effects of the key parameters h, h/l, vs and f_m/f_{1D} on ground motion amplification, each parameter was varied independently while holding the others constant. The average Terrain Amplification Factor (TAF) values for each parameter level were computed and analyzed. As illustrated in Figure 3, the horizontal axis represents the normalized position $x/(b+l)$, where $x/(b+l) = 1$ corresponds to the slope crest, and the vertical axis denotes the TAF. This approach enables a clear assessment of the overall influence of each parameter on amplification, minimizing the impact of outlier values.

Figure 4 (a) demonstrates that the amplification factor increases as the observation point approaches the slope crest, with higher h/l resulting in greater amplification at the top. This is attributed to the intensified multiple reflections and interferences of incident seismic waves within the slope and along its surface as the shape ratio increases. The resulting superposition of wave energy near the crest leads to localized energy concentration and, consequently, a higher amplification factor.

As shown in Figure 4 (b), the amplification factor also peaks near the slope crest across different h. However, variations in slope height have minimal effect on the amplification factor for V-shaped valleys. This is because the amplification is primarily governed by the ratio of slope height to seismic wavelength; when this ratio remains constant, the amplification effect is largely unchanged.

Figure 4 (c) indicates that lower *vs* significantly increase the amplification factor at the slope crest. Reduced shear wave velocity lowers wave impedance, facilitating energy accumulation at the crest. Additionally, shorter wavelengths (associated with lower *vs*) increase the slope height-to-wavelength ratio, enhancing the scattering and interference of seismic waves by the terrain and further intensifying amplification.

Finally, Figure 4 (d) shows that the amplification factor generally increases toward the slope crest for most f_m/f_{1D}. Notably, when f_m/f_{1D}=4 amplification at the valley boundary becomes pronounced, possibly due to wave energy being trapped by damping effects. Overall, as the frequency ratio increases, the amplification effect becomes more significant, with the crest experiencing the highest amplification. When f_m/f_{1D}<1 amplification is negligible, indicating that longer wavelengths interact less effectively with the terrain. In contrast, shorter wavelengths promote strong interactions—such as reflection, scattering, and diffraction—substantially enhancing the amplification effect.

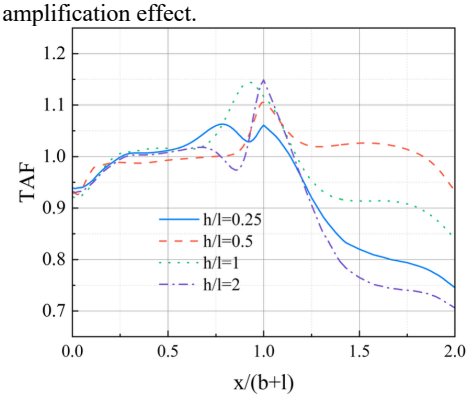

(a) The amplification factor curves under different *h*/*l*

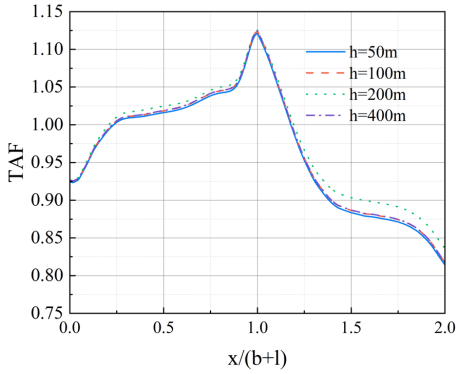

(b) The amplification factor curves under different *h*

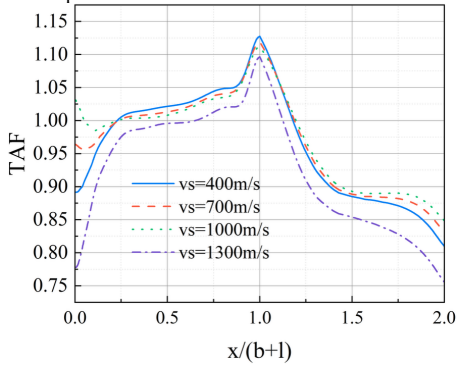

(c) The amplification factor curves under different *h*

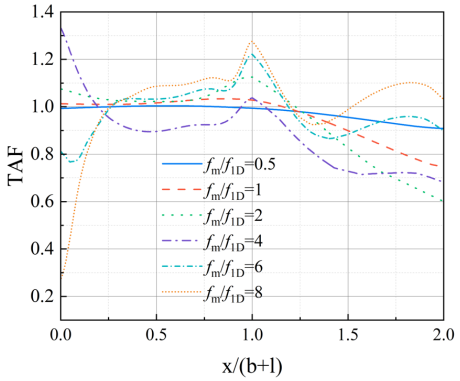

(b) The amplification factor curves under different f_m/f_{1D}

Figure 4. The distribution of magnification coefficients under different influencing factors.

3.2 *Distribution Law of TAF on the surface of the V-shaped site*

According to Figure 4, Areas 1 and 2 exhibit different trends in the variation of the amplification factor: it increases monotonically in Area 1, whereas it decreases in Area 2. Therefore, to facilitate the fitting of the amplification factor expressions and to present the results more clearly, the amplification factor formulation is divided into two parts (Figure 5).

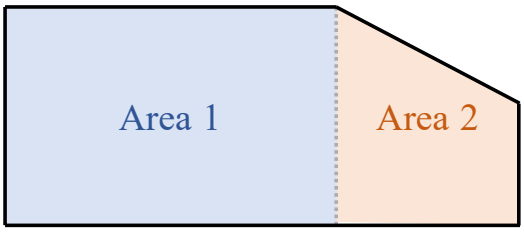

Figure 5. Area 1 and Area 2 of the V-shaped river valley.

As summarized in Table 2, the *TAF* exhibits consistent distribution patterns with respect to variations in *h*, *h*/*l*, *vs* and f_m/f_{1D}. Specifically, in both Area 1 and Area 2, the *TAF* in Area 1 increases, while that in Area 2 decreases, as *x*/*b* and *x*/*l* increase. Given the complex influence of the frequency ratio f_m/f_{1D} on surface *TAF*, the analysis is divided into three frequency bands: 0.5~2, 4, and 6~8. For frequency ratios between 0.5 and 2, the *TAF* in Area 1 increases and in Area 2 decreases with increasing *x*/*b* and *x*/*l*. At a frequency ratio of 4, the *TAF* in Area 1 increases from the midpoint toward both the slope crest and the edge of Area 2, while the *TAF* in Area 2 continues to decrease as *x*/*l* increases. For frequency ratios between 6 and 8, the *TAF* in Area 1 increases with *x*/*b* and in Area 2, it rises from the midpoint toward both the slope crest and the edge of Area 2.

Table 2. Summary of the distribution pattern of TAF.

Influence factor	Range	The TAF distribution in Area 1	The TAF distribution in Area 2
h	50m~400m	(→+)	(→－)
h/*l*	0.25~2	(→+)	(→－)
vs	400~1300	(→+)	(→－)
f_m/f_{1D}	6~8	(→+)	(←→)
	4	(←→)	(→－)
	0.5~2	(→+)	(→－)

Note: (→+) indicates that *TAF* increases as *x*/*b* or *x*/*l* increases; (→－) indicates that *TAF* decreases as *x*/*b* or *x*/*l* increases; (←→)

indicates that *TAF* increases in two segments from the middle to the top and edge of the slope.

4 THE FORMULA FOR THE MAGNIFICATION FACTOR OF A V-SHAPED SITE

4.1 *The Proposal of the Amplification factor Formula*

Building on the distribution patterns of surface TAF identified in Section 3, a polynomial fitting approach was employed to develop amplification factor formulas as functions of the independent variables h, h/l, vs and f_m/f_{1D}. As summarized in Table 3, separate amplification factor formulas were derived for Area 1 and Area 2, categorized by the f_m/f_{1D}, resulting in a total of five distinct expressions. Eq.(6) to (10) are second-order polynomials that incorporate the four key influencing factors, a positional parameter (x/b or x/l), and relevant interaction terms. These formulas enable the estimation of the amplification factor at any surface location, accounting for both geometric characteristics and soil properties.

$$TAF = 0.996097 + 0.046296 \cdot h/l + 0.014616 \cdot f_m/f_{1D} - 0.084431 \cdot x/b - 0.031941 \cdot h/l \cdot x/b + 0.027752 \cdot f_m/f_{1D} \cdot x/b + 0.076395 \cdot (x/b)^2 \quad (6)$$

$$TAF = 1.373598 + 0.087903 \cdot x/b - 0.037686 \cdot (h/l)^2 + 0.027544 \cdot h/l \cdot f_m/f_{1D} - 0.071084 \cdot h/l \cdot x/b - 0.351612 \cdot f_m/f_{1D} \cdot x/b + 1.090307 \cdot (x/b)^2 \quad (7)$$

$$TAF = 0.965567 + 0.019757 \cdot h/l + 0.253094 \cdot x/b - 0.031393 \cdot (h/l)^2 + 0.115450 \cdot (h/l) \cdot (x/b) + 0.119464 \cdot (f_m/f_{1D}) \cdot (x/b) - 0.831270 \cdot (x/b)^2 \quad (8)$$

$$TAF = 1.011171 - 0.089297 \cdot h/l + 0.023083 \cdot f_m/f_{1D} - 0.297321 \cdot x/l + 0.072446 \cdot (h/l)^2 - 0.035664 \cdot h/l \cdot x/l + 0.012417 \cdot (f_m/f_{1D})^2 - 0.013688 \cdot f_m/f_{1D} \cdot x/l + 0.107669 \cdot (x/l)^2 \quad (9)$$

$$TAF = 1.167965 - 0.408313 \cdot h/l - 0.661427 \cdot x/l + 0.152106 \cdot (h/l)^2 - 0.286676 \cdot h/l \cdot x/l + 0.073067 \cdot (f_m/f_{1D}) \cdot (x/l) + 0.451363 \cdot (x/l)^2 \quad (10)$$

Table 3. The magnification factor formulas for Area 1 and Area 2.

The segmented interval of f_m/f_{1D}	The magnification factor formula of Area 1	The magnification factor formula of Area 2
0.5~2	Eq. (6)	Eq. (9)
4	Eq. (7)	Eq. (9)
6~8	Eq. (8)	Eq. (10)

The coefficients of each term in the polynomial represent the relative influence, or weight, of the corresponding factor on the amplification effect. To assess the sensitivity of each parameter, the coefficients from Eq. (11) to (15) were statistically analyzed. As illustrated in Figure 5, the sensitivity ranking of the influencing factors in both Area 1 and Area 2 is as follows: $f_m/f_{1D} > h/l > h > vs$. This analysis demonstrates that seismic wave frequency exerts the greatest impact on the amplification factor among the four factors considered. This indicates that resonance between seismic waves and site geometry is the primary mechanism driving amplification and affecting slope response. Therefore, it is essential to account for frequency effects when evaluating site amplification.

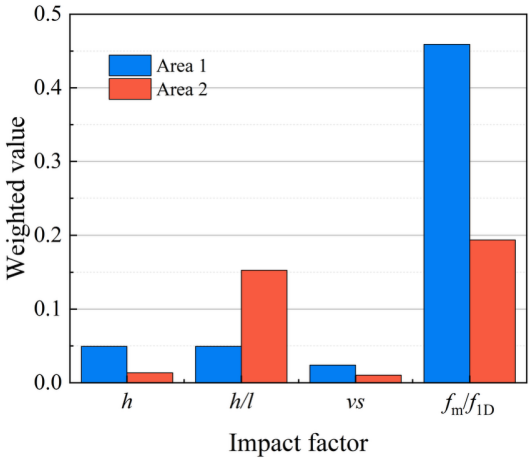

Figure 6. The weights of the magnification factor formulas for Area 1 and Area 2.

4.2 *Verification of magnification factor*

Figure 7, Figure 8 and illustrate the performance of the TAF formula in fitting the original data. The fitted curves closely match the observed data, accurately capturing the underlying trends and demonstrating the effectiveness of the proposed model. Furthermore, Figure 9 presents the linear correlation between the numerical results and the predicted values, with an R^2 value of 0.8939. This high coefficient of determination confirms the statistical reliability and predictive capability of the developed formula.

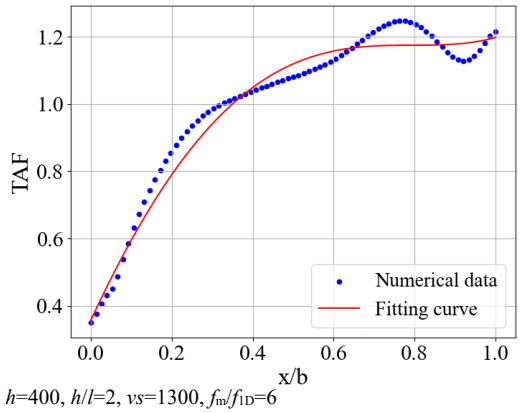

(a) h=400, h/l=2, vs=1300, f_m/f_{1D}=6

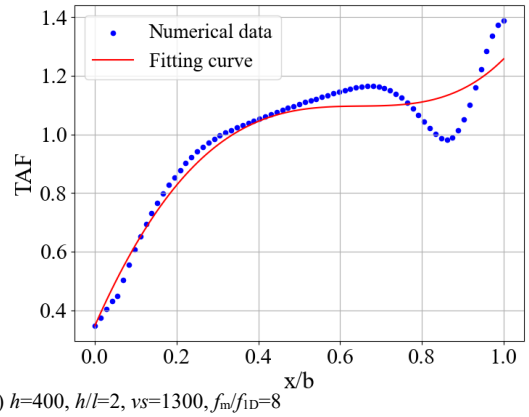

(b) h=400, h/l=2, vs=1300, f_m/f_{1D}=8

Figure 7. The original data and fitting curve of TAF in Area 1.

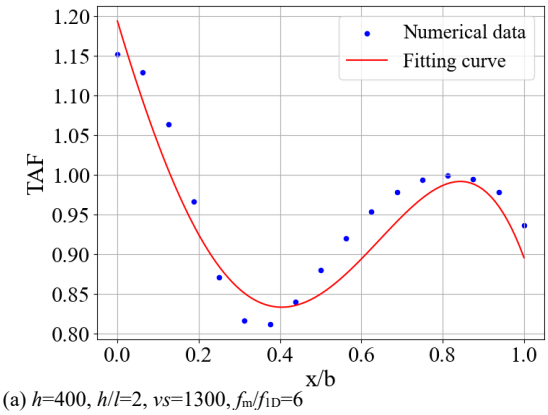

(a) h=400, h/l=2, vs=1300, f_m/f_{1D}=6

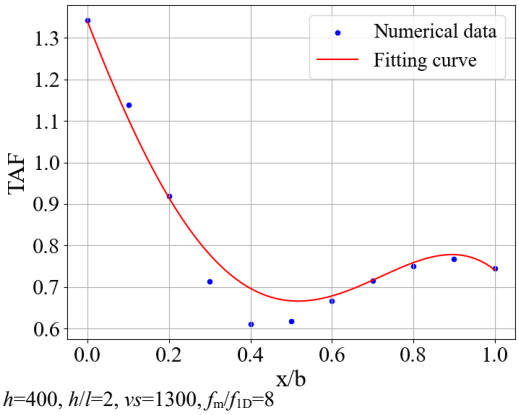

(b) h=400, h/l=2, vs=1300, f_m/f_{1D}=8

Figure 8. The original data and fitting curve of TAF in Area 2.

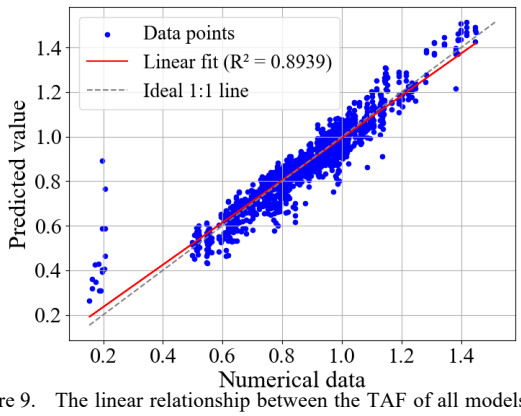

Figure 9. The linear relationship between the TAF of all models and the fitted data.

To evaluate the practical applicability of the TAF formula, real-world data from the Jade V-shaped River Valley (Figure 10) were used for comparison. Based on the parameters reported by (Huang & Chiu. 1995), the site has a width of 1500 m, a depth of 350 m, a medium density of 2.67 g/cm³, and a shear wave velocity of 1500 m/s. As shown in Figure 11, the predicted amplification factor is consistently lower than the observed values, although both exhibit similar trends—specifically, the amplification factor decreases with increasing distance from the valley bottom. The discrepancy arises because the actual site contains soft and weak soil layers, which tend to increase amplification as seismic waves propagate through them. In contrast, the present study focused on Class I and Class II sites with relatively weak nonlinearity, and thus did not account for soil nonlinearity in the model. This omission results in the predicted values being slightly lower than the measured values.

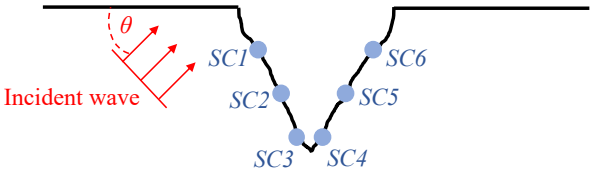

Figure 10. Emerald Valley.

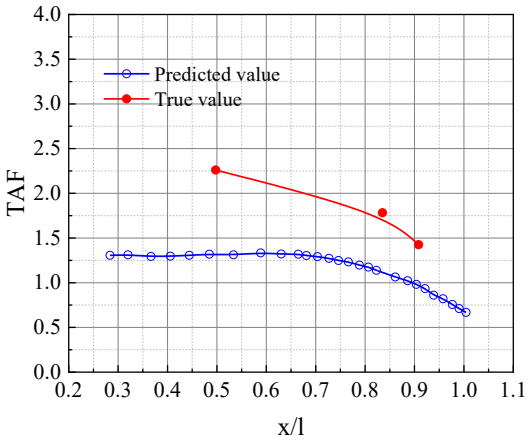

Figure 11. The predicted value of the TAF formula and the true value of Emerald Valley.

5 DISCUSSION

To elucidate the similarities and differences between the numerical results of this study and existing domestic and international standards, as well as to highlight the limitations of current codes regarding the influence of seismic wave frequency, the amplification factor derived herein are compared with those specified in relevant codes.

According to China's (GB50011-2010), the topographic seismic amplification factor for sites with complex terrain is determined by factors such as the terrain height, slope steepness, and the distance from the site to the edge of the protruding terrain. In general, steeper and higher slopes lead to greater amplification effects at the crest, while the amplification decreases as the distance from the slope or crest increases. The code incorporates these parameters into its calculation formula to account for the influence of local topography on ground motion.

Similarly, the European Code (EC-8) stipulates that for sites with slope angles exceeding 15°, the horizontal amplification factor should be selected within the range of 1.2 to 1.4. EC-8 further assumes that this amplification factor decreases linearly with increasing distance from the plateau edge.

As established in Section 3.2, seismic wave frequency significantly affects the site amplification factor. To assess this effect, the TAF values under different f_m/f_{1D} were compared with the standard values prescribed by GB50011-2010 and EC-8. As shown in Figure 11, the amplification factor specified by both codes at each x/b position are generally higher than the average values obtained from the numerical simulations, suggesting that the codes are conservative when frequency effects are not considered. However, at the edge of the V-shaped site, some numerically derived TAF values exceed those specified by the codes. This discrepancy indicates that GB50011-2010 and EC-8 do not fully account for the influence of seismic wave frequency, nor do they consider the amplification or attenuation effects resulting from the complex interactions among reflected, refracted, and surface waves at site edges.

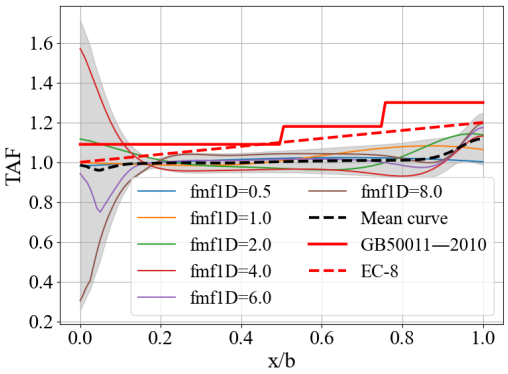

Figure 12. Comparison of amplification factor with standard values at different f_m/f_{1D}.

6 CONCLUSION

- The amplification of ground motion in V-shaped river valleys is most pronounced at the slope crest, and this effect is further intensified by an increased shape ratio, reduced shear wave velocity, and higher frequency ratio. Collectively, terrain geometry, material properties, and seismic wave frequency govern the variation of the amplification factor.
- The proposed TAF amplification factor formula demonstrates strong agreement with numerical simulation results and exhibits robust statistical reliability. While the predicted values for V-shaped valley sites are slightly lower than measured values, the overall trends are consistent, confirming the validity and applicability of the formula for estimating amplification factor on V-shaped terrain surfaces.
- However, the GB50011-2010 and EC-8 standards do not fully account for the influence of seismic wave frequency, leading to potential underestimation or overestimation of amplification factors, particularly at site edges. Among the factors considered, seismic wave frequency exerts the greatest influence on surface amplification. It is therefore recommended that seismic wave frequency be explicitly incorporated into future revisions of seismic design codes.

7 ACKNOWLEDGEMENTS

This work was supported by the National Key Research and Development Program of China (Grant No. 2022YFC3003601), National Natural Science Foundation of China (Grant No. 52478392), Natural Science Foundation of Guangdong Province (Grant No. 2025A1515011857) and Science and Technology Projects in Guangzhou (Grant No. 2025A03J0046).

8 REFERENCES

Eurocode 8, 2000. *ENV 2000—5 Design provisions for earthquake resistance of structures - part 5: foundations, retaining structures and geotechnical aspects*. Brussels: CEN European Committee for Standardisation.

Ministry of Construction of P.R. China, 2010. *GB50011–2010 code for seismic design of buildings*. Beijing, China: China Architecture & Building Press.

Alleanza, G.A., D Onofrio, A., Silvestri, F., 2024. Definition and validation of a valley amplification factor for seismic linear response of 2d homogeneous alluvial basins. *Bulletin of Earthquake Engineering* 22 (11), 5475-5514.

Amini, D., Gatmiri, B., And Maghoul, P., 2022. Seismic response of alluvial valleys subject to oblique incidence of shear waves. *Journal of Earthquake Engineering* 26 (12), 6304-6328.

Assimaki, D., Gazetas, G., Kausel, E., 2005. Effects of local soil conditions on the topographic aggravation of seismic motion: parametric investigation and recorded field evidence from the 1999 athens earthquake. *Bulletin of the Seismological Society of America* 95 (3), 1059-1089.

Ba, Z., Zhao, J., Sang, Q., And Liang, J., 2024. Nonlinear seismic response of an alluvial basin modelled by spectral element method: implementation of a davidenkov constitutive model. *Journal of Earthquake Engineering* 28 (16), 4767-4796.

Cetin, K.O., Zarzour, M., Cakir, E., Tuna, S.C., Altun, S., 2023. 2-d and 3-d basin site effects in izmir-bayrakli during the october 30, 2020 mw7.0 samos earthquake. *Bulletin of Earthquake Engineering* 21 (12), 5419-5442.

Huang, H.C., Chiu, H.C., 1995. The effect of canyon topography on strong ground motion at feitsui damsite: quantitative results. *Earthquake Engineering & Structural Dynamics* 24 (7), 977-990.

Jingbo, L., Xin, B., Shutao, L., Fei, W., Dong, W., 2023. Stability improvement of explicit algorithm when using viscoelastic artificial boundary. *Engineering Mechanics* 40 (05), 20-31.

Kuhlemeyer, R.L., Lysmer, J., 1973. Finite element method accuracy for wave propagation problems. *Journal of the Soil Mechanics and Foundations Division* 99 (5), 421-427.

Li S, Zhang, F., Wang, M., Cheng, Z., Zhang, Y., Zhang, N., Wang, J., Gao, Y., 2022. Seismic response sensitivity of a V-shaped canyon-crossing bridge considering the near-source canyon topographic effects. *Soil Dynamics and Earthquake Engineering* 155, 107205.